Supporting Information

Radiative Pumping and Propagation of Plexcitons in Diffractive Plasmonic Crystals

Yuriy Zakharko[1,3], Marcel Rother[1], Arko Graf[1], Bernd Hähnlein[2], Maximilian Brohmann[1], Jörg Pezoldt[2], and Jana Zaumseil[1*]*

[1]Institute for Physical Chemistry, Universität Heidelberg, D-69120 Heidelberg, Germany

[2]Institut für Mikro- und Nanotechnologie, Technische Universität Ilmenau, 98693 Ilmenau, Germany

[3]Current address: Department of Physics, Technical University of Denmark, 2800 Kongens Lyngby, Denmark

Corresponding Authors

* E-mail: yuriy.zakharko@pci.uni-heidelberg.de, yuzak@fysik.dtu.dk

* E-mail: zaumseil@uni-heidelberg.de

1. METHODS

Sample fabrication, characterization and theoretical analysis.

2. RESULTS

1. Methods

Preparation of CNT dispersion. Monochiral dispersions of (6,5) CNTs were prepared from CoMoCAT® raw material (diameter 0.7–0.9 nm) by selective polymer-wrapping. Poly[(9,9-dioctyluorenyl-2,7-diyl)-*alt-co*-(6,6'-{2,2'-bipyridine})] (PFO-BPy, American Dye Source, M_W = 34 kg/mol) was dissolved in toluene (2 mg/mL) before adding 1.5 mg/mL CoMoCAT material. Next, high-speed shear force mixing (Silverson L2/Air) was applied at maximum speed (10230 rpm) for 72 h at constant temperature of 20 °C. After dispersion, the mixture was centrifuged at 60000 g (Beckman Coulter Avanti J26XP centrifuge) for 1 h. (6,5) CNTs were enriched and excess polymer was removed by vacuum filtration (PTFE filter). The resulting pellet was redispersed in 1 mL of toluene.

Sample fabrication. Nanoparticle arrays on glass substrates were fabricated by electron-beam lithography (EBL) with a Raith 150 system (Raith GmbH) as described previously.[1] Polymer-sorted CNTs were printed with an Aerosol Jet 200 printer (Optomec Inc.), as described previously.[2] The movable sample stage was at 100 °C to enable fast evaporation of toluene. A 200 μm inner diameter nozzle was used at a sheath gas flow of 30 sccm and a carrier gas flow of 15 sccm. Repeated printing cycles of grids were used to achieve a film thickness of 40-50 nm. Samples were completed by spincoating a toluene solution (20 mg/mL) of poly(methyl methacrylate) (PMMA) (M_W = 350 kg/mol, Sigma Aldrich) at 1000 rpm leading to a PMMA layer of 250 nm.

Optical characterization. The absorption spectrum of CNT layer was acquired with a Varian Cary 6000i absorption spectrometer. The photoluminescence-excitation map was obtained by excitation of the CNT film with the wavelength tunable (1 nm step with laser-line tunable filter, Fianium Ltd.) output of a supercontinuum laser source (WhiteLase SC400, Fianium Ltd.) and detection with an Acton SpectraPro SP2358 spectrometer (grating 150 lines/mm) and a liquid nitrogen cooled InGaAs line camera (PI Acton OMA V:1024 1.7). The obtained signal was wavelength calibrated for sensitivity of the detection system and incident laser power (measured with a calibrated silicon photodiode power sensor).

For room temperature reflectance and photoluminescence (PL) spectroscopy, a collimated white light source or circularly polarized laser beam (λ=785 nm; continuous wave power 1 mW, OBIS, Coherent Inc.) was passed through a 50:50 beam-splitter and focused on the sample with a ×100 near IR objective with 0.8 numerical aperture. The back-focal plane of the objective was imaged via Fourier optics and a tube lens onto the entrance slit of a spectrometer (IsoPlane SCT-320, Princeton Instruments) equipped with cooled 2D InGaAs camera (640×512 pixels NIRvana 640ST, Princeton Instruments). Scattered laser light was blocked by a long pass filter with 850 nm cutoff wavelength. An additional polarizer was placed in front of the spectrometer to select transverse-electric or transverse-magnetic light polarization. The reflectivity was defined as the difference between signals from regions on the sample with and without plasmonic crystals divided by the measured spectrum of the lamp.

Simulations. 3D finite-difference time-domain (FDTD) simulations were performed using commercial software (FDTD Solution v8.15.697, Lumerical Solutions Inc., Canada). For the calculation of the local plasmon resonance of a single nanodisk and nanorods (Supporting Information **Figure S2**) a uniform mesh size of 1 nm (X, Y and Z-directions) was used in the region with steep variation of the dielectric function (i.e., around a 25 nm high 165×165 nm gold nanodisk, elliptical 380×180 nm and 620×200 nm nanorods). Outside of these regions the grid was defined by the auto non-uniform mesh technique. The nanodisks/nanorod was placed on the glass substrate and covered by 300 nm PMMA layer (n=1.5 for both). The optical constants of gold were taken from Johnson and Christy.[3] The incoming plane wave was injected normal to the surface and polarized along short or long axis of the nanorods. The calculated difference between power entering and leaving the box power monitor around nanodisks/nanorod is used to deduce the scattering spectrum and thus position of the localized surface plasmons (LSPs).

The field intensity distributions generated by a broadband dipole source in **Figures 2, 4b-d, 5b** were calculated as a difference between the field intensity from the 2D profile monitors (XY and YZ planes) with and without 380×180 nm gold nanorods (on a glass substrate covered by CNT layer and 250 nm PMMA layer, and arranged in the finite 40×20 μm^2 rectangular array with 600×765 nm^2 periodicities). Carbon nanotube layer was represented by the Lorentz oscillator model with dielectric permittivity:

$$\varepsilon_{CNTs}(E) = \varepsilon_{\infty} + \frac{f E_{ex.}^2}{(E_{ex.}^2 - E^2 - i\gamma E)} \quad (1)$$

, where $\varepsilon_{\infty} = 2.45$ is the high-frequency component of the dielectric function, $f = 0.2$ is the Lorentz permittivity, $E_{ex.} = 1.24$ eV is the exciton transition energy and $\gamma = 45$ meV is the exciton line width. These values were adjusted to fit the experimental absorption spectrum in **Figure 1b**.

The far-field projection in **Figure 5d** were calculated from the near-field data recorded by the additional XY 2D power monitor placed above the PMMA layer.[4]

Coupled-oscillator fitting routine. The dispersion properties of the plexcitons were fitted to the eigenvalues of the effective Hamiltonian:

$$H_{PEP} = \begin{pmatrix} E_{ex.} & V_{ex.-LSP} & V_{ex.-DO} \\ V_{ex.-LSP} & E_{LSP} & V_{LSP-DO} \\ V_{ex.-DO} & V_{LSP-DO} & E_{DO}(\theta) \end{pmatrix} \quad (2)$$

, where spectral positon of the localized surface plasmon (LSP) was estimated from the FDTD simulations, i.e., $E_{LSP} = 1.4$ eV (see **Figure S2**). The off-diagonal $V_{ex.-LSP}$, $V_{ex.-DO}$, V_{LSP-DO} coupling strengths were set as the fitting parameters and correspond to the coupling of the excitons or localized surface plasmons to the diffraction order (DO).

For the detection plane along the main crystal axis (at φ=0) the uncoupled angular dispersion for the (0,±1) DO, i.e., $E_{DO}(\theta)$ is of the form:

$$E_{DO}(\theta, \varphi = 0) = \frac{h \cdot c}{a \cdot (n \mp \sin(\theta))} \quad (3)$$

While for the same DO, but at φ=π/2:

$$E_{DO}(\theta, \varphi = \pi/2) = \frac{h \cdot c}{a \cdot \sqrt{n^2 - \sin(\theta)^2}} \quad (4)$$

, where $h \cdot c$ is a product of the Planck constant and the speed of light, a is the array pitch (i.e., 765 nm) and n = 1.5 is the refractive index of environment.

The angle/wavevector-dependent photonic, plasmonic and excitonic fractions (Hopfield coefficients) of the plexciton states (**Figures 1d** and **6a,c**) were calculated via their projection onto the initial uncoupled states.

2. Results

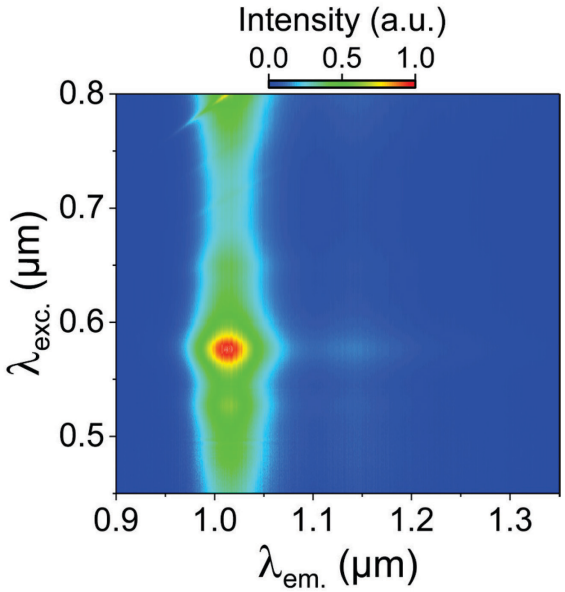

Figure S1. Photoluminescence excitation-emission map of (6,5) CNT layer showing no other emitting CNT species.

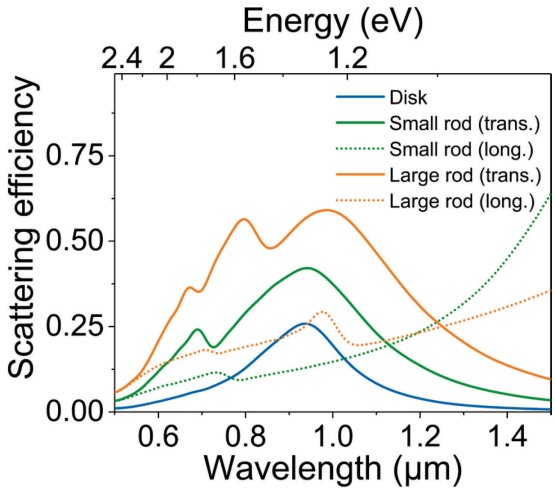

Figure S2. Local plasmon resonances of gold nanodisks and two types of nanorods. FDTD-simulated scattering spectra of D=165 nm gold nanodisks, 380×180 nm (small) and 620×200 nm (large) elliptical nanorods in dielectric environment with n=1.5 along short (transversal, solid) or long (longitudinal, dotted) axis.

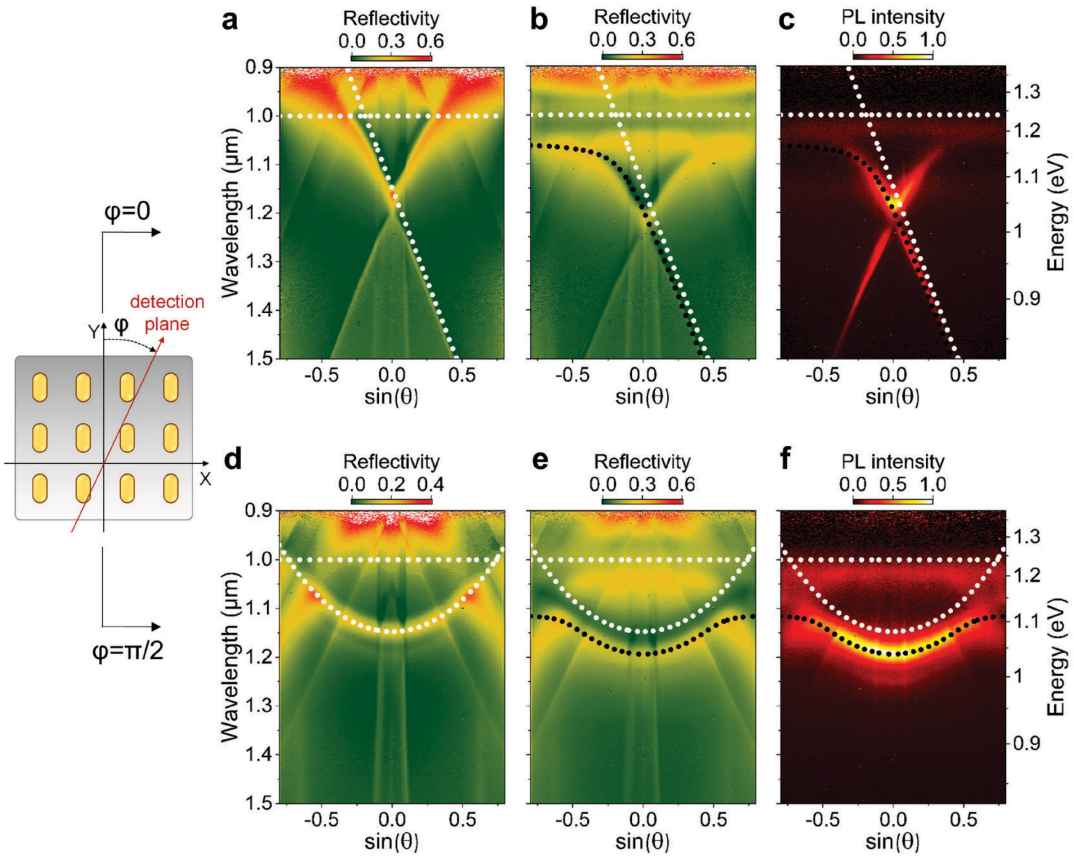

Figure S3. Angular dispersion of sample with large elliptical nanorods (620×200 nm) without (**a**, reflectivity) and with (**b** and **c**, reflectivity and photoluminescence, respectively) (6,5) carbon nanotubes measured along Y-axis. **(d-f)** Corresponding data for detection along the X-axis. White dotted lines indicate bare excitonic (dispersionless) and diffraction order, while the black dotted lines correspond to the fitted plexciton modes.

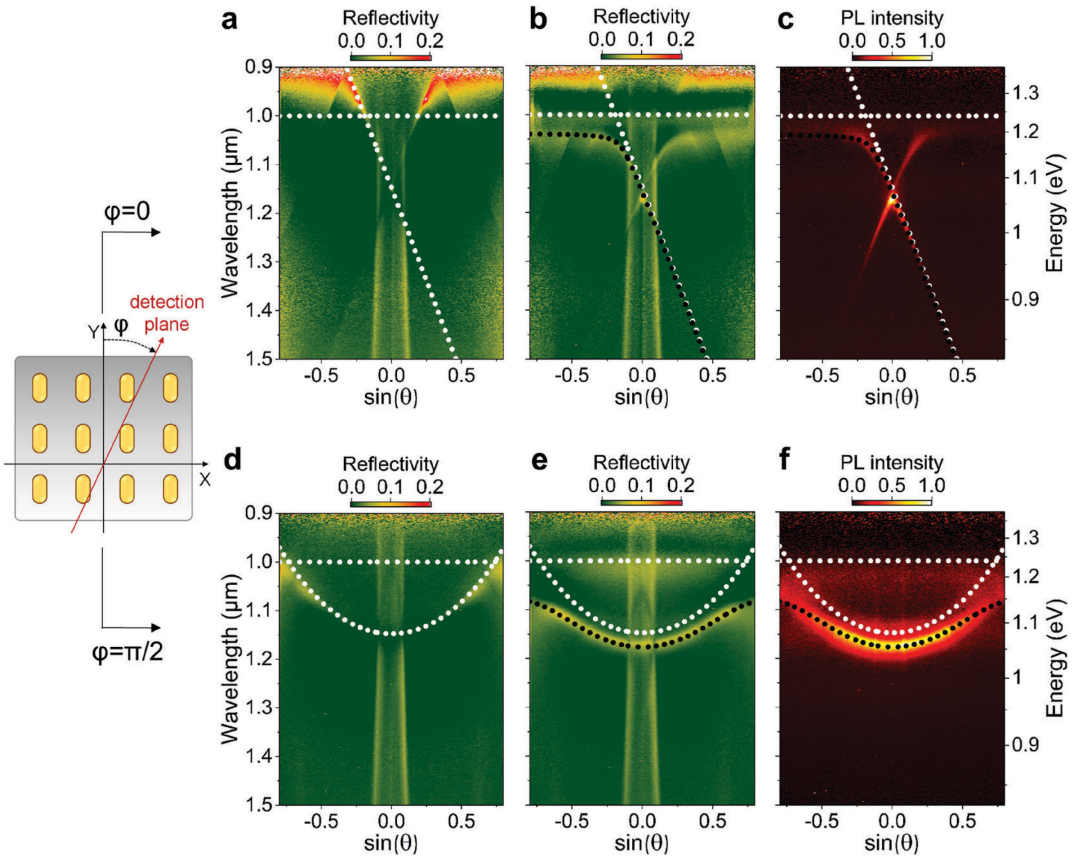

Figure S4. Angular dispersion of sample with nanodisks (D=165 nm) without (**a**, reflectivity) and with (**b** and **c**, reflectivity and photoluminescence, respectively) (6,5) carbon nanotubes measured along Y-axis. **(d-f)** Corresponding data for detection along the X-axis. White dotted lines indicate bare excitonic (dispersionless) and diffraction order, while the black dotted lines correspond to the fitted plexciton modes.

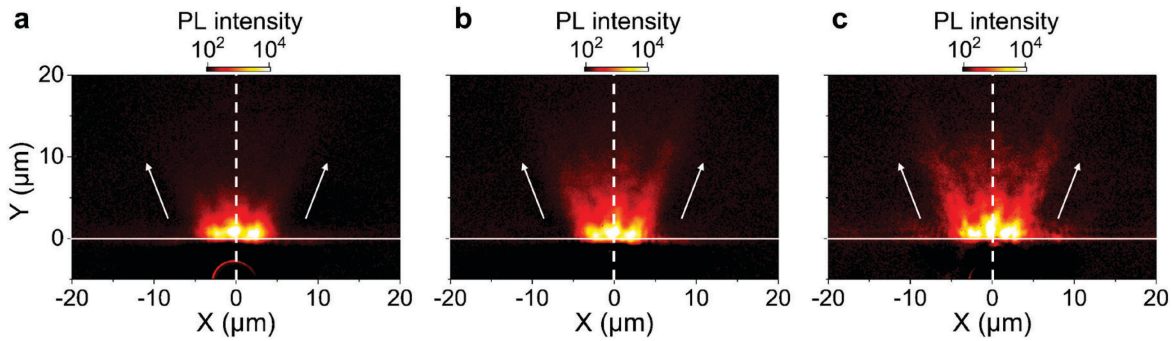

Figure S5. Spectrum-integrated radiative decay and upward propagation of the plexcitons into the plasmonic crystal of large **(a)**, small **(b)** nanorods, and nanodisks **(c)**. Light emission from the region with only carbon nanotubes is subtracted for clarity.

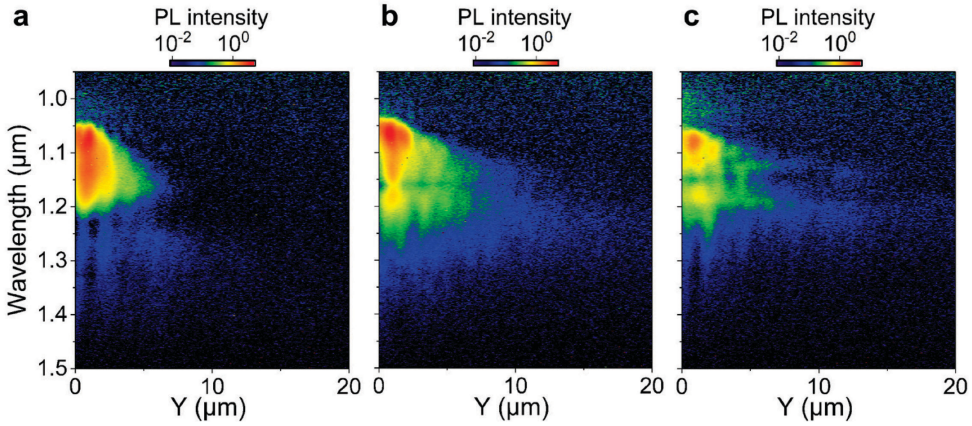

Figure S6. Hyperspectral image of the radiative decay of plexcitons along propagation direction (Y-axis, for X=0 μm) for the plasmonic crystals of large **(a)**, small **(b)** nanorods, and nanodisks **(c)**.

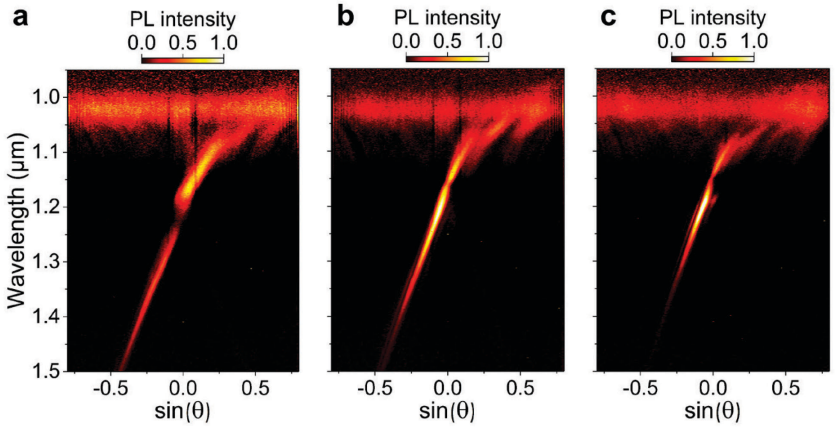

Figure S7. Angular distribution of the radiative decay of plexcitons along propagation direction (Y-axis, for X=0 μm) for the plasmonic crystals of large **(a)**, small **(b)** nanorods, and nanodisks **(c)**.

REFERENCES

(1) Zakharko, Y.; Graf, A.; Schießl, S. P.; Hähnlein, B.; Pezoldt, J.; Gather, M. C.; Zaumseil, J. *Nano Lett.* **2016**, *16*, 3278–3284.

(2) Rother, M.; Brohmann, M.; Yang, S.; Grimm, S. B.; Schießl, S. P.; Graf, A.; Zaumseil, J. *Adv. Electron. Mater.* **2017**, *3*, 1700080.

(3) Johnson, P. B.; Christy, R. W. *Phys. Rev. B* **1972**, *6*, 4370–4379.

(4) https://kb.lumerical.com/en/solvers_far_field_projections.html (accessed April 10, 2018)